Review article

The Micro-Air-Vehicle *Golden Snitch* and Its Figure-of-8 Flapping*

Lung-Jieh Yang

Department of Mechanical and Electromechanical Engineering, Tamkang University, Tamsui, Taiwan 251, R.O.C.

Abstract

Relaxing from the conventional regarding of the rigid flapping mechanism, in this review paper the author introduced flexible wing frames for micro-air-vehicles (MAVs) with the wing span of 20 cm at Tamkang University. The constructed flapping MAV *Golden Snitch* with a smallest body mass of 5.9 g created a successful 107 s flight record with a four-bar linkage driving mechanism in 2008. Augmented by the precision injection molding (PIM) manufacture, the almost polymer-made MAV with the modified driving mechanism increases the flight endurance up to 480 s in 2010. Via high speed photography, the author has ever found the wing-tip trajectory as an oblique figure-of-8 which composes the original up-and-down flapping and the induced coherent streamwise vibration while the wingbeat frequency being about 10–25 Hz. The time-averaged lift, thrust coefficients and the structure aging of MAVs have been investigated to mention the corresponding influence. This figure-of-8 was done by the aero-elastic interactive nature as well as the symmetry-breaking of a simple flapping system. The bifurcation (duality) phenomenon of the oblique figure-of-8 was shown. How the rigidity of the flexible wing frame influences the flapping appearance was also addressed qualitatively. The flexible MAVs exhibited the peculiar figure-of-8 away from the conventional domain of MAVs by the perspective of scaling laws. Some remaining technical issues or future works of the figure-of-8 flapping were summarized finally.

***Key Words*:** Figure-of-8, Micro-Air-Vehicle (MAV), Flexible Wing, Simple Flapping, Four-Bar Linkage, Symmetry Breaking

1. Introduction of Flapping MAVs

The flight mechanism of natural vertebrates and insects fascinated scientists and engineers for centuries [1]. People tried to figure out the mystery buried inside and used the knowledge to develop new generations of air vehicles. The author in this review article surveyed many prior works and introduced the flapping MAV developed at Tamkang University in recent years as well.

One persistent obstacle in the research for unsteady flow mechanisms is the difficulty in directly measuring the aerodynamic forces produced by a flapping bird or insect [2]. A free-flying butterfly has ever been attracted into a wind-tunnel, and an unconventional lift-generating mechanism has then been found *in-situ* [3]. In addition, a MEMS micro force sensor using capacitive detection was developed for characterizing the flight behavior of a tethered fruit fly *Drosophila melanogaster* [4]. MEMS pressure sensors were also mounted on butterfly wings to measure the pressure field in real-time manner [5]. Recently images of the wake vortices of bats *Glossophaga soricina* were analyzed by means of a digital particle image velocimetry (DPIV) method [6]. The detailed 3D trajectory of the flapping honeybee has ever been monitored by a high-speed visual motion sensing or

*This review article is the extension of the author's conference paper presented in the Proc. of the 47th AIAA Aerospace Science Meeting, Orlando, Jan. 5-8, 2009 with the paper no. of AIAA 2009-0875.

*Corresponding author. E-mail: Ljyang@mail.tku.edu.tw

stereo photography framework on the ground [7]. Even more, people controlled the flight motion of a moth [8] or a beetle [9] by implanted neuro-probes. Generally speaking, the researchers of the above works studied the unsteady flow mechanisms by observing living natural flyers. Although the prior flight information is firsthand and precious, two shortcomings are still inevitable. First, living natural flyers are hard to control. Constrained by the man-made environment with limited fidelity, the measured gestures of the living animals are even questioned with their reality. Second, these experimental data from the same species of animals are usually without good repeatability. Therefore the corresponding summary of the flight behaviors or mechanisms is hard to conclude from the massive experimental data of natural flyers.

Several groups developed their flapping MAVs with different configurations and actuation principles after 2000. Caltech's *Microbat* created a 6-min flight record of flapping MAVs using MEMS process and the titanium-parylene material system [10]. TU Delft's MAV *Delfly* composed of a pair of dragonfly-like flexible wings also demonstrated their successful hovering [11]. Otherwise, a fixed-wing type MAV with a scissor-like clapping tail thruster made by Naval Graduate School showed its long endurance of 20 min [12,13]. The MEMS group at Tamkang University presented a flapping wing capable of exporting the on-site lift information through its PVDF wing sensor [14] and the afterward MAV *Golden Snitch* [15]. In 2011, the AeroVironment Inc. announced the successful hovering flight of a 16 cm-span nano-air-vehicle (NAV) *Hummingbird* sponsored by Defensive Advanced Research Project Agency (DARPA) fulfilled the surveillance mission [16,17]. Therefore, these successful artifacts deserved people to investigate their aerodynamic forces and kinematic motions, like the research way of living animals just mentioned before. The advantageous merits of this approach are not only the precise control on the dimension but also on the adjustability of flight parameters, for instance, freestream velocity, angle of attack, wingbeat frequency and so on. By this way the flight information obtained from MAVs with successful flight records could be as references comparable to natural flapping animals, and gave useful guidelines to the development of next generation MAVs in an empirical manner. Based on the observation of these prior works about flapping MAVs, a framework system of research and development was shown in Figure 1. It consists of the gear-transmission mechanism design and manufacture, flapping wing design and manufacture, system assembly and weight reduction compromise, wind-tunnel test, flight test, flight stability and control, and computational fluid dynamics.

As the first step toward constructing the complete framework in Figure 1, it's usually to adopt the scaling laws [18] of natural flyers to relate the body mass m with the wingspan b and the wingbeat frequency f as follows.

$$b = (1.17) \cdot m^{0.39} \tag{1}$$

$$f = (3.98) \cdot m^{-0.27} \tag{2}$$

Take the example of a 0.2 m-span MAV (b = 0.2), the body mass m cannot surpass 0.011 Kg, and the wingbeat frequency f must be faster than 15 Hz. Hence designing and fabricating the key mechanism component of a light flapping MAV is not easy. In other words, the

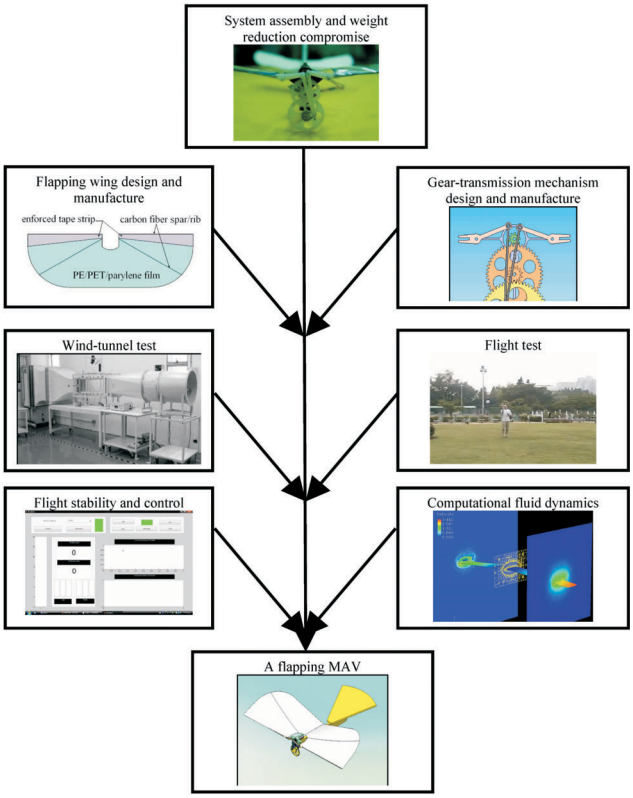

Figure 1. The framework system of research and development for a flapping MAV.

gear transmission mechanism for flapping motion should be as tiny and light as possible in design; the corresponding wingbeat frequency should be also fast enough at the same time; most important of all, the flapping gesture ought to mimic the natural flyers accordingly.

Several sophisticated mechanisms of flapping wings were claimed to fit this natural maneuver motion in the conceptual design, for instance, the researchers in Delaware University employed a 5-bar mechanism for generating a prescribed wing motion taken from a hawk moth kinematic flight data [19]. They additionally designed a mechanism for biaxial rotation of a wing for a hovering MAV [20]. Meanwhile, an insect-like flapping wing mechanism was proposed by Cranfield University through the novel idea of a double spherical Scotch yoke [21,22]. Although these flapping mechanisms with multiple degrees of freedom (DOFs) enabled the flapping vehicle to animate the motion of wing folding [23] or even the ideal horizontal figure-of-8 of hummingbirds [1,18]. These mechanism designs were too complicated to be miniaturized.

In this work the author described how to use the conventional four-bar linkage mechanism to fabricate an ultra-light driving mechanism for wing flapping [15]. The out-of-plane motion termed herein as "oblique figure-of-8" from the original simple flapping will be induced by the flexible wing frame [24,25].

2. Construction of Flapping MAVs

The author's group firstly purchased some key components and fabricated a flapping MAV named as *Eagle-II* with wing span of 30 cm and body mass of 11 g [26]. The best successful flight record of *Eagle-II* is 11 s; the schematic operation of the flapping wing is shown as Figure 2. This MAV is composed of a Balsa-wood wing frame and a set of gear-reduction transmission components, and deposited with conformal parylene film on the wing frame as the airfoil skin by ourselves. The actuation force or torque available for the flapping wings is drained from the gear-reduction transmission set coupled to a high-speed dc pager motor powered by a commercial poly-lithium battery.

The author's group employed a four-bar linkage concept to design the gear transmission mechanism of our MAVs with only one DOF flapping motion for the excuse of very light weight and low technical complexity. Figure 3 shows the three-dimensional view and the four-bar linkage module with gear transmission of the MAVs using in this study. The DIDEL electrical motor is 6 or 7 mm-diameter to drive the gear transmission system. The gear reduction ratio of 26.6 was designed for providing sufficient flapping frequency of 15 Hz subject to the dc motor speed of 24,000 rpm. The whole gear set and the motor were arranged on a plastic or an aluminum holding case. The driving linkage could perform a full

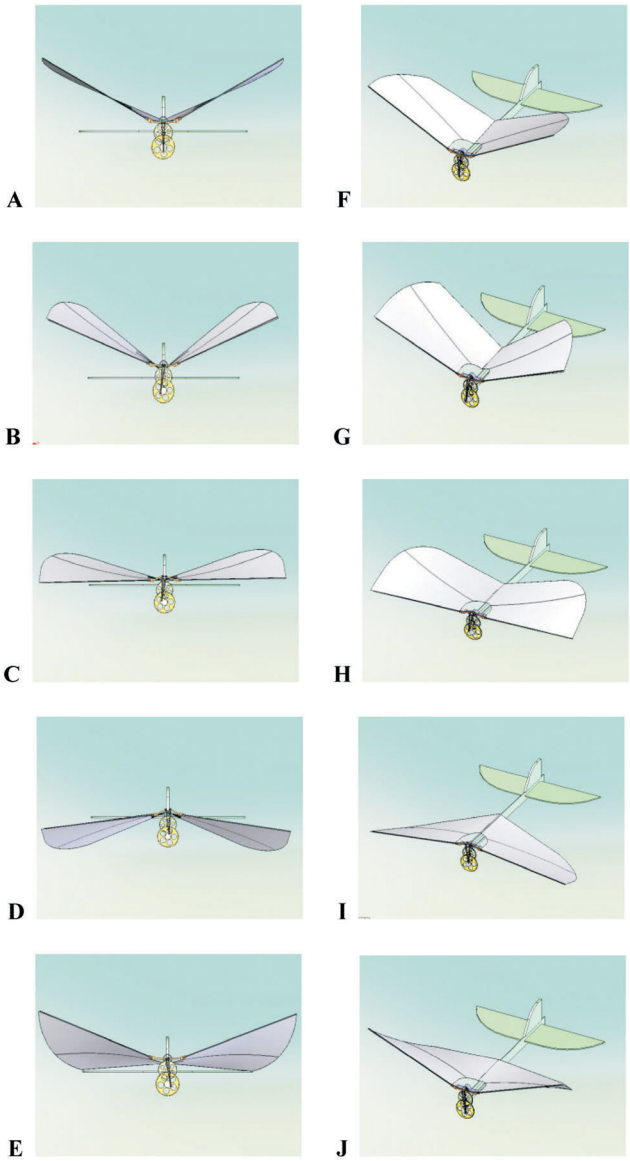

Figure 2. The supposed cartoon of the continuous full-cycle flapping motion of the MAVs with a rigid four-bar transmission module: (A) denotes the neutral position. (B) and (C) denote the down-stroke. (D) and (E) denote the up-stroke. The bird views from (F) to (J) [15] are corresponding to the front side views from (A) to (E), respectively.

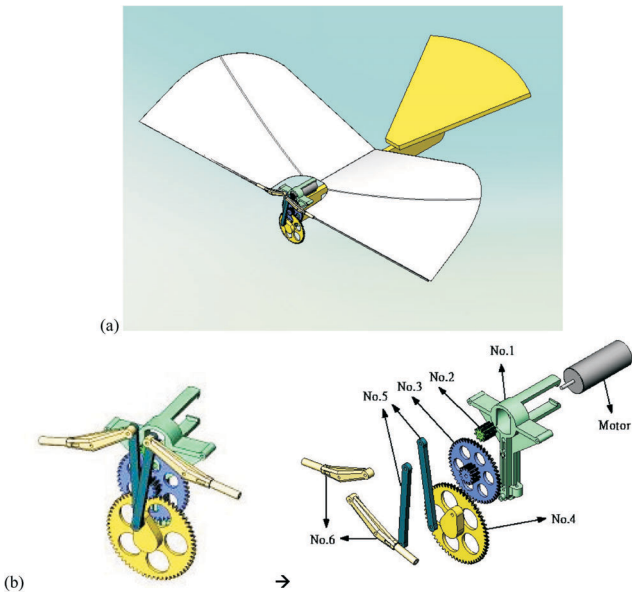

Figure 3. The MAV with a presumed rigid four-bar transmission module: (a) denotes the 3-D view; (b) denotes the four-bar linkage/gear transmission module and its decomposing parts; No. 1 is the holding case or base; No. 2, No. 3, and No. 4 are the speed-reduction gears; No. 5 and No. 6 are the transmission bars. The leading edge bar of the wing frame would be connected to No. 6 bar [15].

revolution and the follow-up linkage governing the wings undergoes a rocking motion.

It should be mentioned in advance that the wing skin was made of parylene foil and be clued to the Balsawood leading edge beams with a simple supported boundary condition instead of a clamped boundary condition. As a result the wing skin that can be rotated freely according to the up-and-down plugging and the instantaneous angle-of-attack of the flapping wing could almost have a simple harmonic motion. In such a way of operation, the flapping wing has the partial capability of flapping and twisting synchronously. In other words, the simple flapping mechanism herein basically animates the natural flyers of the prior literature [2]. It's therefore possible to generate the unsteady flow mechanisms including delayed stall, wake capture, and rotation circulation through flapping and provide the necessary aerodynamic forces accordantly.

3. Wind Tunnel Test of the Semi-Rigid MAV *Eagle-II*

The aerodynamic performance of the MAV *Eagle-II* was firstly studied before the real flight. In the flapping ground test, the flapping frequency or the wingbeat frequency ω was controlled by the DIDEL dc motor and the voltage applied to it. This aerodynamic force measurement was conducted in a wind-tunnel at the freestream speed U of 0.4–3.0 m/s, measured by a hot-wire anemometer. The turbulence intensity of the wind tunnel flow field was evaluated as 0.05–0.028%, far below the suggested value of 1% by Mueller [27]. In addition, the authors measured the blockage ratio defined as the ratio of the cross section area of the MAV and the wind tunnel. Referring to the Ref. [28], the wall effect can be neglected if the blockage ratio is less than 7.5%. The recommended AOA of the installed MAV less than 30° is free from the wall effect for the wind tunnel here.

The load cell (Bertec, OH, USA) with force specifications of 200 gf and 100 gf was responsible for the force measurement of lift L and the net thrust T, respectively. The net thrust force T here is defined as the thrust force minus air drag. The present load cell has the maximum error 0.2% of the full-scale signal due to nonlinearity or hysteresis. In the wind-tunnel testing, the MAV was installed on the load cell directly to obtain the data of lift and net thrust forces [29]. The author demonstrated a set of classical time-varying force signals of lift and net thrust as shown in Figure 4 [30]. For clarification, this force history behaved obviously unsteadily.

Because the unsteady aerodynamic investigation was quite different from the conventional case of steady aerodynamics, an important dimensionless parameter of so-called "advance ratio" should be introduced here. The equation (3) defined advance ratio J as the ratio of the freestream velocity U to the maximum speed in the flapping direction, i.e. [10]

$$J = U / b\omega\phi \tag{3}$$

where the flapping speed equals the multiplying product of wing span b (= 25 cm), wingbeat frequency ω (= 7.2–15.7 Hz), and flapping stroke angle ϕ (= 35°). The J value approaches to infinity for the case of fixed-wings; on the contrary, J is less than 1 for the general unsteady flapping flight.

The lift and net thrust coefficients C_L, C_T (divide lift L and net thrust T with dynamic pressure and wing area respectively give lift coefficient C_L and net thrust coeffi-

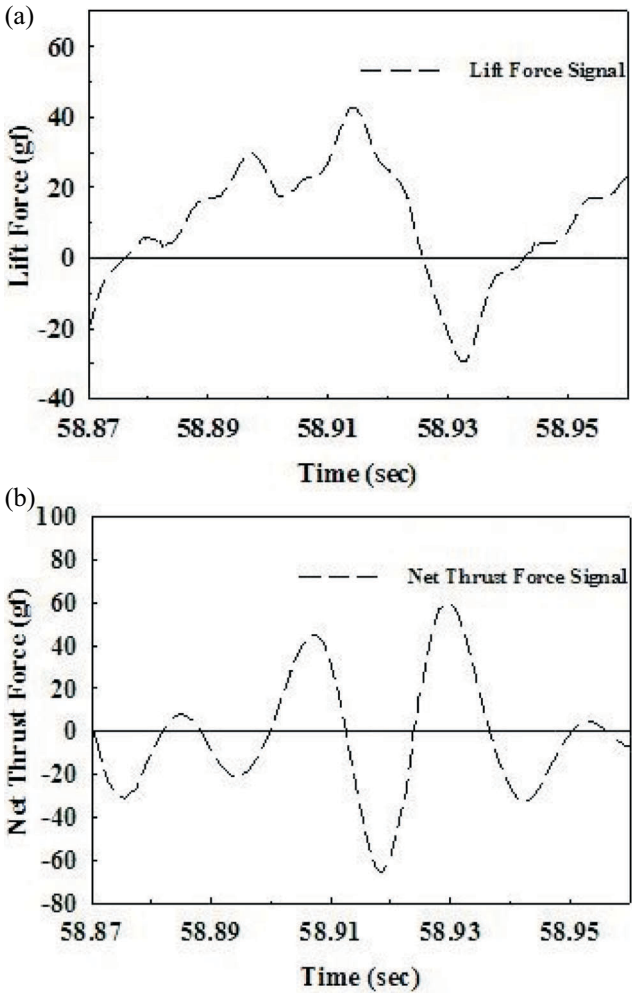

Figure 4. The classical signals of unsteady aerodynamic force with a flapping frequency of 15.4 Hz: (a) lift; (b) net thrust [30].

cient C_T with respect to a certain advance ratio J) extracted from a wind-tunnel test of the MAV *Eagle-II* with a semi-rigid leading edge subject to a fixed angle-of-attack of 20° and different advance ratios are shown in Figure 5.

The scheduled process of collecting a data point in Figure 4 was defined as Ref. [30]. The data-breeding rate of the load-cell was set as 1,000 points per second. The author collected 12,000 points of data in every flapping condition, and processed them into time-averaged values of lift L and net thrust T in Figure 5. In general, these time-averaged lift coefficient C_L of the MAV larger than 3.0 in the regime of J below 0.4 resembled the enough counterbalance force to the weight of the MAV. The net thrust coefficient C_T subject to J value below 0.4 was always positive also denoted the continuous forward pushing without speed decreasing during the real flight.

However, after a certain period of operation time the thrust data in the small advance ratio or high flapping-frequency region of $J < 0.4$ in Figure 5 revealed the trend of diversity or data fluctuation. Such a diversity of thrust data was traced back and suspected from the irregular operation of the worn gear transmission module. In other words, the wear of the power transmission mechanism impeded the smooth flapping and induced the corresponding unpredictable aerodynamic forces. Figure 6 shows the detailed four-bar (black dash line) gear transmission module for the MAV *Eagle-II*. The seriously worn (reaming) portion is specifically marked with a red circle for the Balsa leading-edge frame (and the motor is removed in the figure). This kind of reaming on the Balsa wood not only denotes an aging issue against good

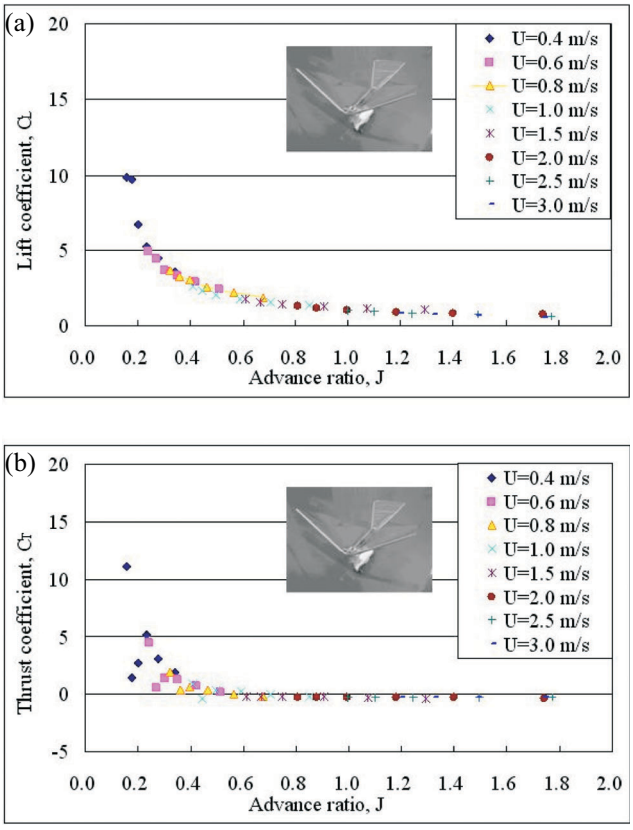

Figure 5. The aerodynamic coefficients of the MAV *Eagle-II* with parylene film of 20-30 μm thick, and b = 25 cm; ω = 7.2–15.7 Hz; ϕ = 35°: (a) Lift coefficient C_L and (b) net thrust coefficient C_T versus advance ratio J corresponding to different freestream velocities U [14]. The net thrust values of U = 0.4 and 0.6 m/s have serious problem of unpredictable data fluctuation.

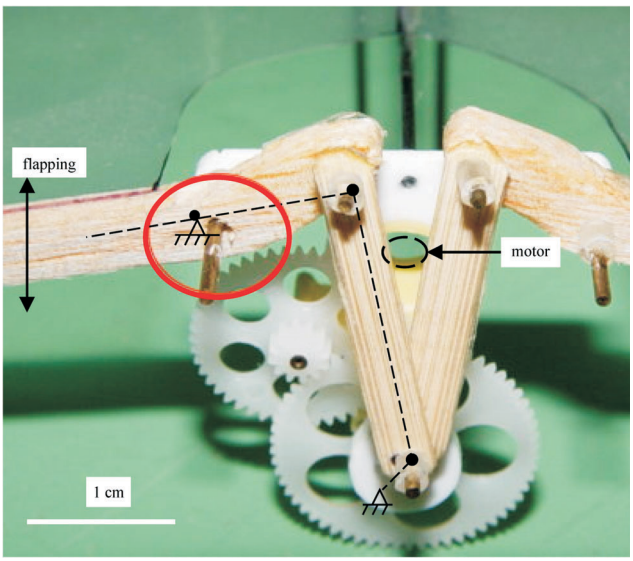

Figure 6. The four-bar (black dash line) gear transmission module for the MAV *Eagle-II*. The seriously worn portion is marked with a bold circle for the Balsa leading-edge frame.

life-time of our MAVs but also reveals a certain uncommon penalty force resulting from the improper matching of the semi-rigid wing structures into our simple flapping mechanism.

4. The Modified Flapping MAV *Golden Snitch*

The Knoller-Betz effect of thrust generation by means of a simply up-and-down flapping was observed in 1909 [31] and 1912 [32]. For the conventional rigid symmetric wing with very large bending moment of inertia, the corresponding thrust force cannot react with apparent forward deformation on the whole wing structure. Additionally, the exact time location of the biggest thrust during a flapping cycle has not been pointed out precisely by the Knoller-Betz effect. Under the constraint of the almost rigid wing frames, there seems no way but to design a complicated flapping mechanism to follow the 3-D flapping trajectory like hummingbirds or even having the trajectory of "clap-and-fling" [33] like insects for the artificial winbeating vehicles. In that conventional thinking of mechanism design, too much flexibility of the wing frames means the operation failure or malfunction of the flapping machines mimicking the biological gesture of natural flyers.

The opposite design methodology in this study, on the contrary, is to use the much lighter and more flexible materials as the key structures for the new version of MAVs. For instance, the author's group shortened the wing span from 25 cm to 20 cm toward the miniaturization trend. The correlated body mass regulated from the scaling law of birds equation (1) [18] is no more than 11 g. For the light weight consideration, the author replaced the Balsa-wood leading edge frame with fine carbon-fiber rods. Meanwhile, the aluminum-alloy four-bar gear transmission module is re-constructed by the electrical-discharging wire cutting (EDWC) [15]. The new power transmission module made of aluminum alloy shown in Figure 7 reduces greatly to 1.2 g in mass, far less than the case of 2.8 g for Caltech' *Microbat* [34]. This above belief or revelation from small technology is that the more miniaturized artifacts may render us with better structural stiffness and operation life time.

The author's group remodeled the MAV with the new flexible wing frames and the new gear transmission module mentioned above, kept reducing the total weight and wing span, and finally obtained the modified MAV named as *Golden Snitch* with wing span of 20 cm and body mass of 5.9 g in Figure 8. The aerodynamic coefficients versus advance ratio J for the MAV *Golden-Snitch* were measured as Figure 9. The scheduled process of

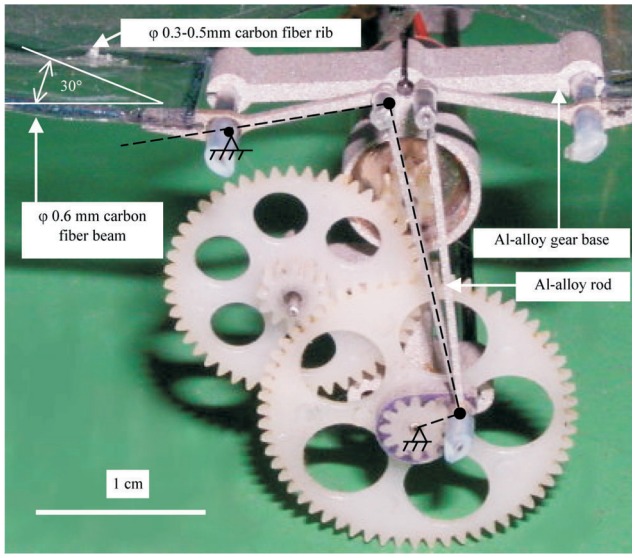

Figure 7. The weight-reduced four-bar (black dash line) gear transmission module for the MAV *Golden Snitch*. The leading-edge beam is made of 0.6 mm-diameter carbon-fiber beams and aluminum-alloy bars. A rib with 30° back-swept to the leading edge beam is optionally installed. All the tiny aluminum parts were precisely manufactured by EDWC [15].

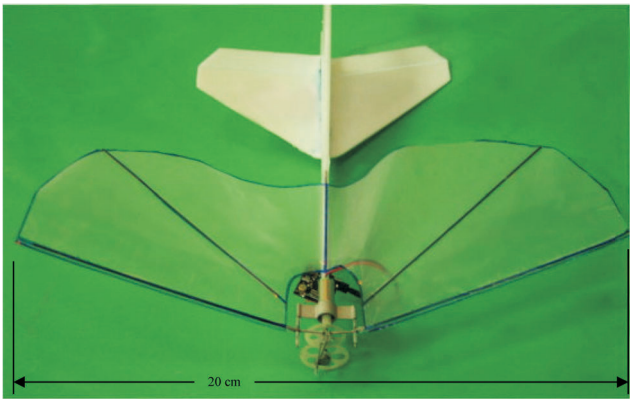

Figure 8. The completed MAV *Golden Snitch* with the carbon-fiber leading-edge beam/rib and parylene skin. A 7 mm-diameter electrical motor mounted in the newly developed aluminum-alloy holder with the new transmission module of Figure 7 is actuated by a poly-lithium battery of 30–50 mAh. The total mass including flexible wing frame, motor, gear assembly, wing, fuselage, tail, battery and receiver is only 5.9 g.

collecting data in the wind-tunnel testing is the same as the case of *Eagle-II*. The new testing results of aerodynamic performance effectively improve the thrust data with 35% increasing in magnitude, and moreover without the previous issue of unpredictable data fluctuation. The disappearance of the structure reaming or aging on pivoting joints prevented lots of friction loss and may benefit the real flight of our new MAVs. Furthermore, with this great decrease of friction loss in the mechanical transmission module, the wingbeat frequency of the MAV *Golden Snitch* can exalt to 20 Hz or even much faster than before.

The new MAV *Golden Snitch* equipped with new configuration and characterized with light weight and high flexibility has a far more outstanding flight performance than the semi-rigid *Eagle-II*. With scarcely real-time adjustment by remote control *Golden Snitch* actually made a successful flight record of 107 s, breaking the 11 s record of *Eagle-II* to a great extent in 2008. Without the negative effect of side gust wind, *Golden Snitch* would like to fly roughly along the virtual barrel surface of an imaginary cylindrical column with a diameter of several meters. The author's group has additionally succeeded in two folds of precision injection molding (PIM) manufacture for making the polyoxymethylene (POM) gear transmission module and the expandable polystyrene (EPS) fuselage for the *Golden*

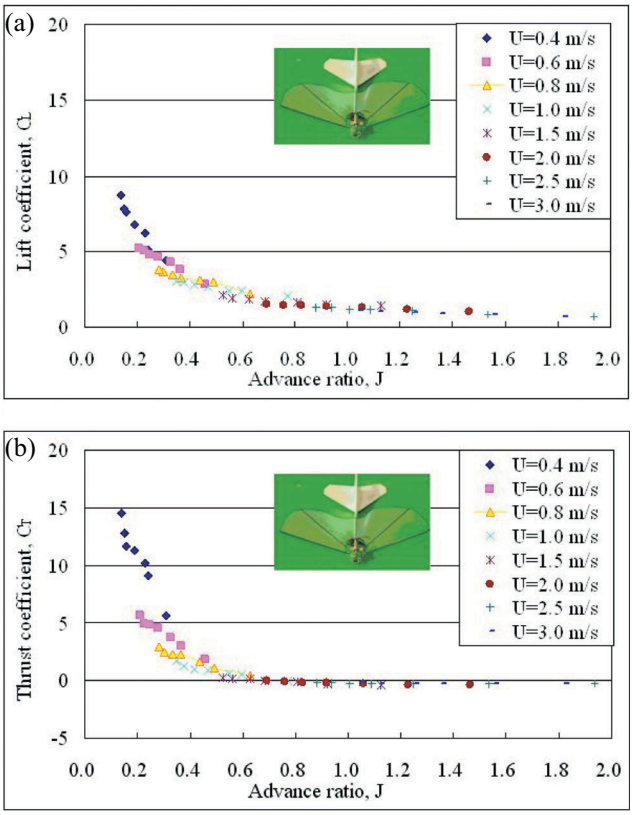

Figure 9. (a) Lift coefficient C_L and (b) net thrust coefficient C_T of the MAV *Golden-Snitch* versus advance ratio J corresponding to different freestream velocities U (b = 20 cm; $\phi = 38.9°$; $\omega = 10.5$-23.6 Hz.)

Snitch-Pro shown in Figure 10 [35].

Three improvements of Figure 10 over the author's prior arts have been achieved: (1) the flight endurance has extended to 480 s in 2010; (2) the fabrication time using PIM is only 1 min, much shorter than 30 min by EDWC; (3) the landing times of *Golden Snitch-Pro* could safely land for 100 times with the protection of EPS fuselage [35].

5. Oblique Figure-of-8 Flapping of MAV *Golden Snitch*

Thanks to the intrinsically flexible wing structure of *Golden Snitch* herein, this MAV exalts in free flight without much energy losing in resisting against the surrounding air. The author luckily found that a streamwise vibration of the carbon-fiber leading edge was characterized by wingbeat frequency from 15.6 to 21.7 Hz for the wings with 30°-ribs. That frequency was much smaller than the natural frequency of 85 Hz for the wing struc-

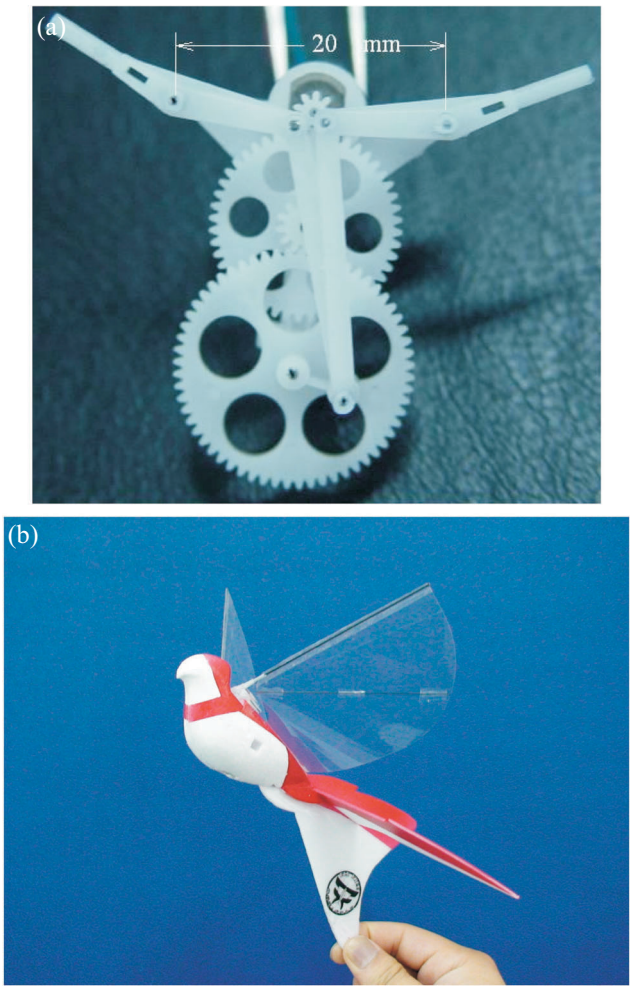

Figure 10. Tamkang's *Golden Snitch-Pro* in 2010: (a) the assembled plastic gear transmission module; (b) the implemented product model [35].

ture. It meant that this special vibration had no matter with the resonance of the wing frame. By combining this induced coherent streamwise vibration of the wing frame and the vertical reciprocating flapping motion in Figure 2, a 3-D figure-of-8 flapping motion of the MAV obviously showed up and could be seen even by human naked eyes. This streamwise vibration of the wing frame was originated from the fore mentioned Knoller-Betz effect [31,32] and interpreted as a coherent forward locomotion.

The ordinary video camera with 30 frames of images per second only provides too slow speed for depicting detailed viewgraphs of a full-cycle flapping kinematics. The continuous blinks of the figure-of-8 trajectory of the wing tip were then taken and certificated by a high speed CCD camera (Phantom v. 4.2) for the MAV *Golden Snitch* in quiet ambient. The author installed this MAV in the wind-tunnel and captured the real-time images of the flapping wings subjected to two cases with and without the 30°-rib respectively in Figure 11.

The surface morphology of the wing skin showed the wavy profile from the leading edge to trailing edge and from the wing tip to inner wing root simultaneously, which accorded the supposed flexible wing design with a sinusoidal change of the leading-edge angle-of-attack. More additionally, the author verified the similar phenomena of figure-of-8 flapping for the MAV *Golden Snitch* subjected to different freestreams velocity which is set from 0.4 to 3.0 m/s.

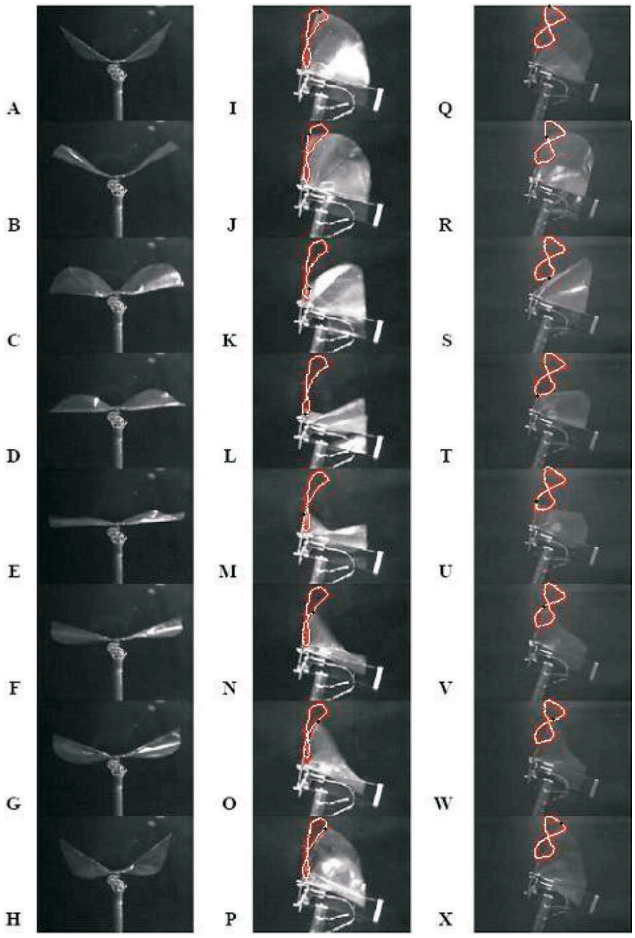

Figure 11. The high-speed continuous full-cycle blinks of *Golden Snitch*'s flapping wing. The front side views from (A) to (H) are corresponding to the side views without rib from (I) to (P), and to the side views with 30°-rib from (Q) to (X). The angle of attack is 20° (frequencies are about 9.4–25 Hz for the no-rib wing and 15.6–21.7 Hz for the stiffened 30°-rib wing.)

6. Symmetry Breaking and Bifurcation of the Figure-of-8 Flapping

According to the genetic design aspects of flapping vehicles, the structures of the wings of small natural flyers had rigid leading edges and soft, flexible trailing edges. The leading edge should be hard to bend but easy to twist [36]. The trailing edge of the MAV *Golden Snitch* was made of parylene or other polymer films and agreeable to the flexible requirement of the above rules of thumb. The leading edge carbon-fiber beam was also easy to twist but vulnerable to the bending along streamwise or up-and-down directions, however. The bending of the leading edge due to large wind loading or high-frequency flapping on the one hand resulted in a lag in sustaining leading edge vortices in-time for lift generation and therefore somewhat weakened the unsteady mechanism of "delayed stall". On the other hand the coherent locomotion [37,38] of the elastic leading edge created the figure-of-8 flapping, and made up for the previous lift loss by other unsteady mechanisms, e.g., "wake capture" or "rotational circulation" [2].

Due to some chaotic reasons, e.g., the duality of bifurcation [37,38], the figure-of-8 contours didn't match with an identical trajectory. Their geometry related the winbeat frequency genuinely. The author collected some classical figure-of-8s of the MAV *Golden-Snitch* and evaluated the width-to-height ratios (W/H) versus wingbeat frequency in Figure 12.

On the issue of non-identical figure-of-8 contours, the author would like to address the horizontal moving of a 2-D vertically oscillating plate foil in fluid [37]. That ideal case of a vertically-oscillating plate broke its symmetry in dynamics and started to move forward or backward freely. The forward or backward speed coherently matched linearly with the original oscillating frequency, but a hysteresis or bifurcation existed intrinsically. In more clear words, the oscillating frequencies for starting and ending the forward/backward locomotion were not the same. The above issue has been theoretically investigated, too [38]. Compared to these prior studies, the flapping MAV in this work could be regarded as a non-ideal but a more complicated case. The wing frame was very flexible, and the airfoil was not symmetric at all. Therefore the flow field was 3-D, not like the 2-D case in Vandenburghe's work, and composing of more physical contents in fluid mechanics. The author conducted two arguments in the following:

(1) The issue discussed in Vandenburghe's work was the ideally simplified model of the MAV with the figure-of-8 flapping. It took for granted that the figure-of-8 flapping would gradually disappear if the flexible MAV increasing its rigidity of the wing frame structure. This argument has been somewhat explained by Figure 12. From Figure 12, a corresponding frequency window of the figure-of-8 flapping did exist for a specific wing frame with certain flexibility. More qualitatively, a more flexible wing frame (the case of the no-rib wing) owned a wider range of frequency (9.4–25 Hz) with a smaller lower limit. Consequently to the very extreme case, no frequency window of the figure-of-8 flapping belonged to an ideally rigid (zero flexibility) wing frame.

(2) The figure-of-8 flapping in this study should implicitly comprise all the characteristics mentioned in the

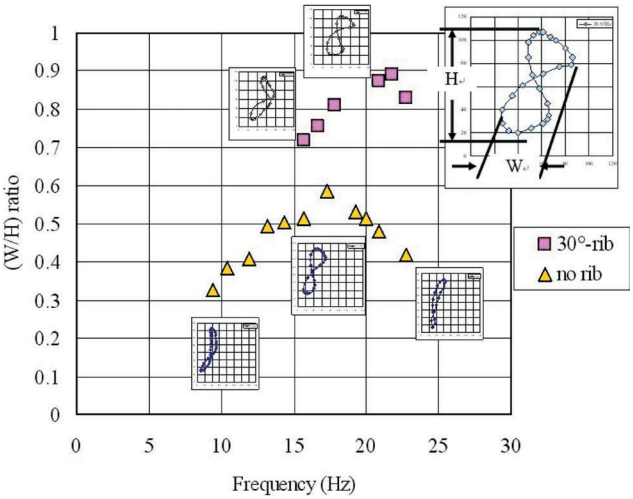

Figure 12. The width-to-height ratios of some figure-of-8 trajectories, extracted from the high-speed CCD images, of the MAV *Golden-Snitch*'s subjected to different wingbeat frequencies corresponding to the no-rib wing and the stiffened wing with a 30°-rib in quiet ambient (no freestream velocity). The width and height are defined as W and H in the figure. The width-to-height ratio is regarded as the equivalent parameter to the propulsive thrust or forward locomotion in real flying. For the 30°-rib wing, the (W/H) ratios around 0.81 ± 11% depict the similar traces at all wingbeat frequencies except that the lower loop is bigger than the upper loop at high speed region. For the no-rib wing, the (W/H) ratios around 0.46 ± 28% denote the much larger variation in the figure-of-8 traces with different speeds.

ideal model of Vandenburghe's work, of course including the bifurcation phenomena. Figure 13 demonstrated the figure-of-8 trajectories for the MAV *Golden Snitch* with the voltages increasing and decreasing between 3.7 and 0.9 V. Even under the same voltage of driving, the winbeat frequency of the voltage-increasing case was no larger than the voltage-decreasing case except the maximum voltage case. The author furthermore collected the wingbeat frequency versus the driving voltage subject to the figure-of-8 flapping in Figure 14(a). The starting wingbeat frequency of showing the figure-of-8 (13.51 Hz) was larger than the frequency which the figure-of-8 disappeared (9.62 Hz). The pathway of a complete up-and-down operation loop depicts the duality of bifurcation. The width-to-height ratio of the figure-

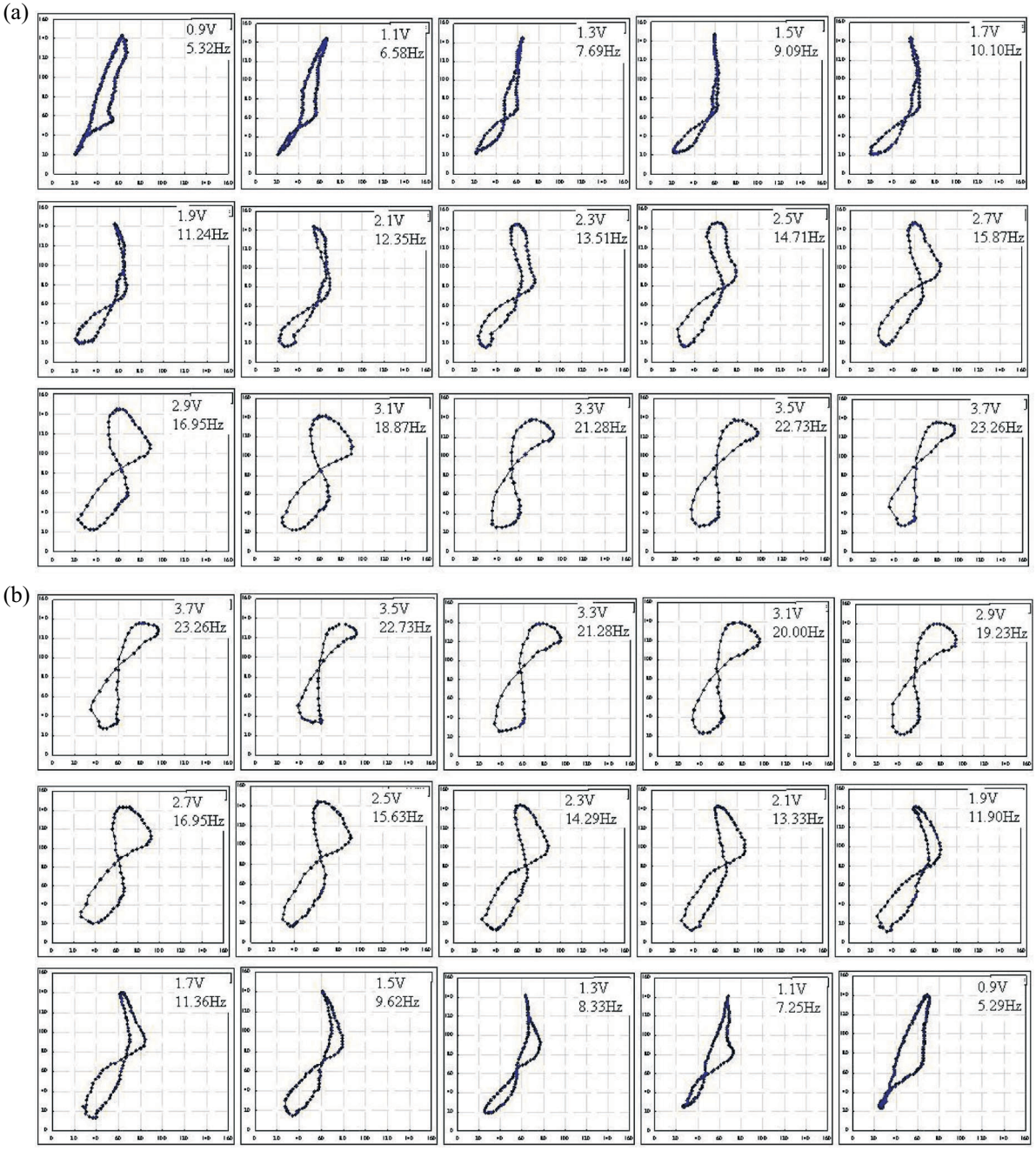

Figure 13. The trajectories of figure-of-8s for the MAV *Golden Snitch* with different driving voltages from 0.9 V to 3.7 V: (a) the voltage-increasing case; (b) the voltage-decreasing case.

of-8 versus different wingbeat frequency is plotted in Figure 14(b) as well. Herein the width-to-height ratio of the figure-of-8 acts as an equivalent index of coherent locomotion like the rotating frequency or the driven Reynolds number in Vandenburghe's work [37].

7. Analogous Relationship in Scaling Laws for Flapping Flyers

Rather than depicting the anatomical analysis on the wing frames of flapping flyers, herein the authors preferred to categorize the MAV with figure-of-8 flapping into some animal groups and conventional MAVs according to their realistic wing spans and the wingbeat frequencies with respect to different body masses. Based on Norberg [18] and Shyy's collecting information [39], the denoting spots of the MAVs *Eagle-II* (wing span = 25 cm, body mass = 11 g, wingbeat frequency = 16Hz) and *Golden Snitch* (wing span = 20 cm, body mass = 5.9 g, wingbeat frequency = 20 Hz) in this work were inserted into the previous plots of wing-span versus body-mass as Figure 15 and winbeat-frequency versus body-mass as Figure 16. The structural limit and the aerodynamic limit in Figure 16 were mentioned in Refs. [18,38–43]. *Eagle-II* was still allocated on the margin of conventional MAVs and small natural flyers, while *Golden Snitch* with figure-of-8 flapping approached to the characteristic region of hummingbirds. Apparently the inductive remark on this observation come to that *Golden Snitch* here might have biomimetic relationship with hummingbirds due to the common property of figure-of-8 flapping, even though the inclined gesture of the flapping plane for these two flyers were quite different. With such an encouraging finding, the domain of MAVs marked as the shadow region in Figures 15 and 16 extended from body

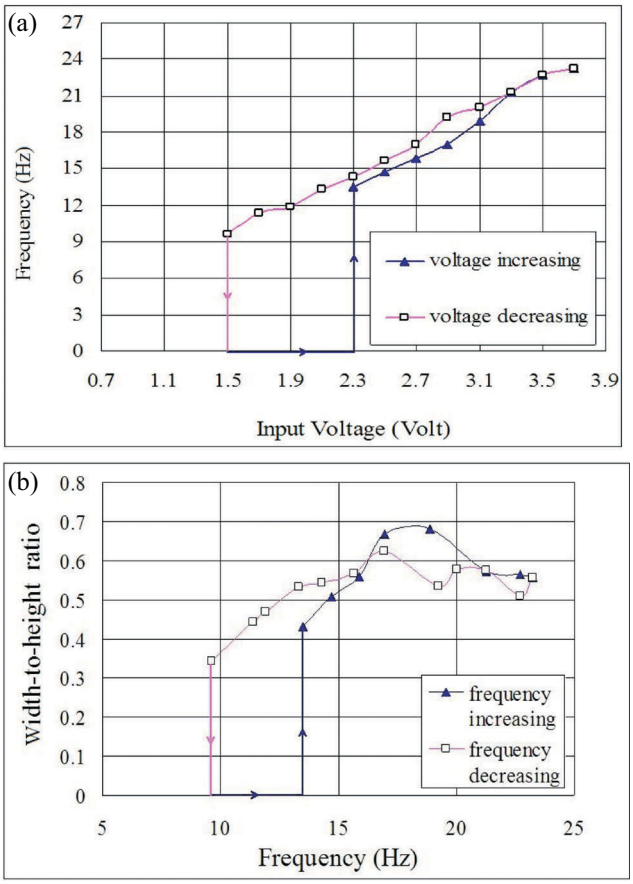

Figure 14. The bifurcation or the hysteresis phenomena of the flexible wing installed on the MAV *Golden Snitch*: (a) the flapping (wingbeat) frequency versus input driving voltage according to voltage-increasing and decreasing cases; (b) the forward locomotion effect or the width-to-height ratio of the figure-of-8 of the flexible wing.

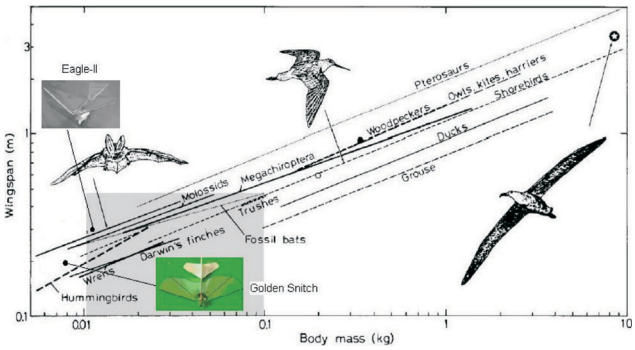

Figure 15. Wing span plotted on logarithmic coordinates against body mass for some animal groups [18], conventional MAVs (shadow region [38–43]), and the MAVs (*Eagle-II* and *Golden Snitch*) in this work.

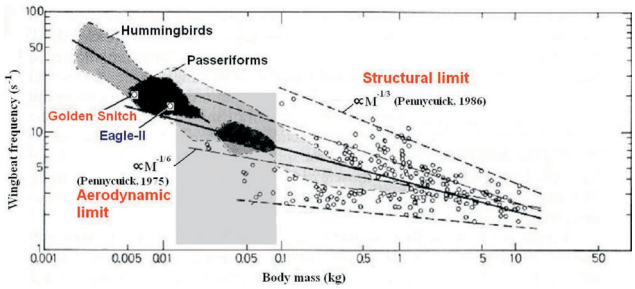

Figure 16. Winbeat frequency (or flapping frequency) versus body mass for some animal groups [18], conventional MAVs (shadow region [38–43]), and the MAVs (*Eagle-II* and *Golden Snitch*) in this work [15].

mass of 11 g down to 5.9 g by this study.

No matter how the author followed the empirical design formulae deduced from hummingbirds, the figure-of-8 flapping is verified empirically and necessary to design a MAV which can fly successfully with wing span less than 20 cm and body mass below 10 g. Subjected to this design requirement of the artificial novel figure-of-8 flapping, a flexible wing frame driven by a single DOF, four-bar linkage mechanism was provided as the neatest design so far as people know. In this work or the practice manner, the cross section of the leading edge carbon-fiber beam was suggested to be round, and the natural frequency of this leading edge beam should be so much larger than the wingbeat frequency without structural resonance as to sustain a successful coherent vibration out from the flap-sweeping plane due to the in-plane pushing forward by the periodic vigorous thrust.

Restated, by the observation of the biologic fact that almost flying or swimming animals often have flexible wing structures, an artificial flying vehicle designed with flexible wing frames did actually adapt itself to any instantaneous change of its air flow environment [39]. Herein the MAV *Golden Snitch* manifested the above flexible characteristic even though its actuation was only originated from a simply flapping mechanism.

8. The Future Technical Issues of Flapping MAVs

The technical issues regarding flapping MAV systems are broad and complex. In general there are unsteady aerodynamic force measurement by windtunnel, 3D kinematic motions of the flapping wings, the unsteady computational fluid dynamic computation (CFD), and even more the particle image velocimetry (PIV) flow visualization technique. The author tried to summarize a potential research framework of flapping MAVs without using PIV in Figure 17 and briefly mentioned as follows.

The aerodynamic force measurement of a flapping MAV in a wind tunnel has the intrinsic difficulty of decomposing the propulsive thrust and the air drag. In the author's experience, the net thrust defined as the thrust minus the drag is the more convenient information obtained directly from the wind tunnel force gauge [14, 15,30]. The afterward application of the measured aerodynamic information including the time history of lift and the net thrust forces should be accommodated in the next paragraph.

How to capture the detailed 3D trajectory of flapping wing motion is still prevailing [7,24,44,45]. The more questionable viewpoint is that how to access the bountiful information to develop promising models for flapping wings. Therefore the unsolved communicative path (a) in Figure 17 denotes deriving the wingtip trajectory by a proper kinematic model using wind tunnel data [46,47]. The emerging modeling methodology, for example of the oblique figure-of-8 flapping herein, needs the fore mentioned time history of lift and net thrust as the time-varying external forces in the momentum equation and needs the real stiffness values (in other words, Young's modulus multiplied with the moment of inertia) of the flapping wings as the input parameters [30,48–50].

The unsteady CFD studies for flapping wings are massive and full of challenges [51–55]. It's not easy and time-consuming to directly solve the fluid-structural problem solely by the Navier-Stokes equations and the elasticity equations of force equilibrium in a coupled manner. An unsolved communicative path (b) in Figure

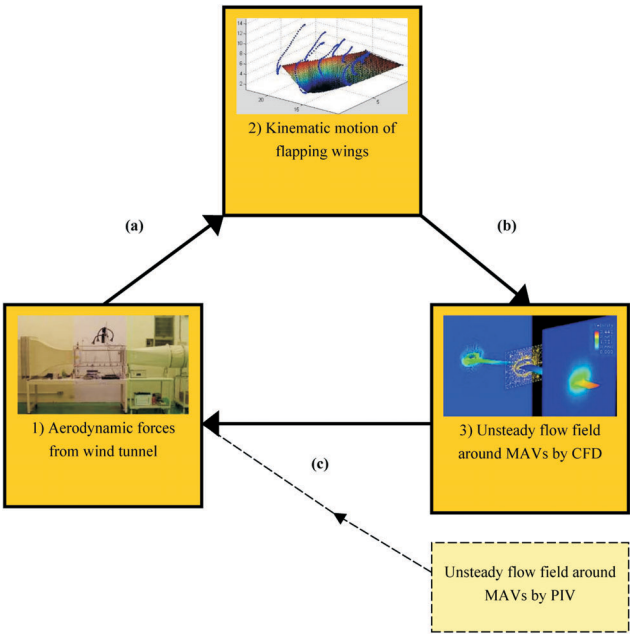

Figure 17. The potential research framework of flapping MAVs by the author: path (a) denotes comparing the wingtip trajectory by a proper kinematic model using wind tunnel data; path (b) denotes providing the 3D moving wing boundaries for CFD simulation; path (c) denotes integrating the pressure field around MAVs to obtain the aerodynamic forces numerically.

17 hence denotes the measured 3D time-varying wing trajectory via stereo photography can be regarded as the 3D moving wing boundaries for CFD simulation [24]. Thereafter the researchers can focus more on finding the nonlinear flow characteristics buried inside without solving the coupled elasticity problems of the wing frame structures.

The technique of PIV flow visualization is of course exquisite and powerful to determining the flow fields around flapping MAVs [6,56,57]. This can be regarded as an alternative or ultimate measurement system comparable to the above 1)-2)-3) triangle framework in Figure 17. The PIV data and the CFD output both need the straightforward communicative path (c) of pressure field integration to interpret the resultant aerodynamic forces on the flapping wing [54,55,57] so as to be compared to the wind tunnel data.

One manifestation of the research framework in Figure 17 to flapping MAVs herein is how the lift and thrust forces influenced by the oblique figure-of-8 phenomenon quantitatively. In the future the real-time, synchronized lift and thrust forces will not only be compared to the smoke track in the wind tunnel, but also compared to the unsteady flow field stimulated by CFD. More quantitative analyses of the lift and thrust versus the width-to-height ratio of figure-of-8 flapping are of course expected to be further investigated as well.

9. Conclusion

In summary, the passive design aspect of improving the performance of the wing frames for flapping MAV *Golden Snitch* introduced in this paper tends to provide a simpler flying platform with moderate gear-transmission module but to produce bountiful and interesting phenomena. This leaded to the decreasing of the vehicle weight and increasing of the endurance of the MAV, and the time-averaged thrust was also increased 35% in magnitude. With the help of a high-speed camera, the figure-of-8 trajectories of the MAVs' wing tips were confirmed by their proper function of the carbon-fiber wing frames and the parylene wing skin. The non-degenerate unsteady lift data and the highly enhanced thrusting locomotion acquired from the wind-tunnel testing did great contribution to the successful flight of the MAVs, even the embedded unsteady flow mechanism still needs more theoretical explanations. This work also removed the technical barrier against the designers in making complicated multi-DOF actuating mechanisms for generating figure-of-8 flapping. The author additionally proposed Vandenburghe's coherent locomotion of the forward flapping motion as the fundamental model of our MAV with figure-of-8. The qualitative influence of the rigidity of wing frames on the frequency window as well as the bifurcation phenomena has been addressed. Finally, with the advantage of light weight and size miniaturization, the author demonstrated an extension of the existing MAV domain. It's believed that this neatest design methodology for flapping MAVs will be not only promising in practice, but the correlated kinematic motion of the figure-of-8 or the theoretical investigation of the solid-fluidic interaction also deserves follow-up attentions.

Acknowledgements

The author is grateful to the financial support from National Science Council of Taiwan with the project numbers of NSC 96-2221-E-032-013/014, 97-2221-E-032-015/016, and 98-2221-E-032-025-MY3. He also thanks the experimental helps from many colleagues and students at Tamkang University: Prof. S.-W. Kang, Prof. F.-Y. Hsiao, Dr. C.-K. Hsu, Mr. I.-C. Huang, Mr. M.-W. Gao, Mr. C.-Y. Kao, and Mr. H.-C. Chen. The discussions with Prof. Y.-C. Tai of Caltech, Prof. A.-B. Wang of National Taiwan University, Prof. J.-M. Miao of National Pingtung University of Science and Technology, Prof. Y.-K. Shen of Taipei Medical University, and Prof. C.-K. Huang of Lunghua University of Science and Technology are highly acknowledged as well.

References

[1] Sane, S. P., "The Aerodynamics of Insect Flight," *The Journal of Experimental Biology*, Vol. 206, pp. 4191–4208 (2003).

[2] Dickinson, M. H., Lehmann, F. O. and Sane, S. P., "Wing Rotation and the Aerodynamic Basis of Insect Flight," *Science*, Vol. 284, pp. 1954–1960 (1999).

[3] Srygley, R. B. and Thomas, A. L. R., "Unconventional Lift-Generating Mechanisms in Free-Flying Butterflies," *Nature*, Vol. 420, pp. 660–664 (2002).

[4] Sun, Y. and Nelson, B. J., "MEMS Capacitive Force

Sensors for Cellular and Flight Biomechanics," *Biomedical Materials*, Vol. 2, pp. s16–s22 (2007).

[5] Takahashi, H., Matsumoto, K. and Shimoyama, I., "Measurement of Differential Pressure on a Butterfly Wing," *Proceedings of the 23rd IEEE International Conference on MEMS*, Hong Kong, pp. 63–66 (2010).

[6] Hedenström, A., Johansson, L. C., Wolf, M., von Busse, R., Winter, Y. and Spedding, G. R., "Bat Flight Generates Complex Aerodynamic Tracks," *Science*, Vol. 316, pp. 894–897 (2007).

[7] Zhang, G., Sun, J., Chen, D. and Wang Y., "Flapping Motion Measurement of Honeybee Bilateral Wings Using Four Virtual Structured-Light Sensors," *Sensors and Actuators A: Physical*, Vol. 148, pp. 19–27 (2008).

[8] Tsang, W., Stone, A., Aldworth, Z., Otten, D., Akinwande, A., Daniel, T., Hildebrand, J., Levine, R. and Voldman, J., "Remote Control of a Cyborg Moth Using CNT-Enhanced Flexible Neuroprosthetic Probe," *Proceedings of the 23rd IEEE International Conference on MEMS*, Hong Kong, pp. 39–42 (2010).

[9] Sato, H., Berry, C. W., Peeri, Y., Baghoomian, E., Casey, B. E., Lavella, G., VandenBrooks, J. M., Harrison, J. F. and Maharbiz, M. M., "Remote Radio Control of Insect Flight," *Frontiers in Integrative Neuroscience*, Vol. 3, p. 24 (2009).

[10] Pornsinsirirak, T. N., Tai, Y. C., Nassef, H. and Ho, C. M., "Titanium-Alloy MEMS Wing Technology for a Micro Aerial Vehicle Application," *Sensors and Actuators A: Physical*, Vol. 89, pp. 95–103 (2001).

[11] Barrett, R., McMurtry, R., Vos, R., Tiso, P., De Breuker, R., Barrett, R., McMurtry, R., Vos, R., Tiso, P. and De Breuker, R., "Post-Buckled Precompressed (PBP) Elements: A New Class of Flight Control Actuators Enhancing High-Speed Autonomous VTOL MAVs," *Proceedings of SPIE - The International Society for Optical Engineering*, Vol. 5762, pp. 111–122 (2005).

[12] Jones, K. D., Bradshaw, C. J., Papadopoulos, J. and Platzer, M. F., "Bio-Inspired Design of Flapping-Wing Micro Aerial Vehicles," *Aeronautical Journal*, Vol. 109, pp. 385–393 (2005).

[13] Rozhdestvensky, K. V. and Ryzhov, V. A., "Aerodynamics of Flapping-Wing Propulsors," *Progress in Aerospace Sciences*, Vol. 39, pp. 585–633 (2003).

[14] Yang, L. J., Hsu, C. K., Ho, J. Y. and Feng, C. K., "Flapping Wings with PVDF Sensors to Modify the Aerodynamic Forces of a Micro Aerial Vehicle," *Sensors and Actuators A: Physical*, Vol. 139, pp. 95–103 (2007).

[15] Yang, L. J., Hsu, C. K., Han, H. C. and Miao, J. M., "A Light Flapping Micro-Aerial-Vehicle Using Electrical Discharge Wire Cutting Technique," *Journal of Aircraft*, Vol. 46, pp. 1866–1874 (2009).

[16] Information on http://www.avinc.com.

[17] "The 50 Best Inventions," *Time*, Nov. 28, p. 80 (2011).

[18] Norberg, U. M., *Vertebrate Flight: Mechanics, Physiology, Morphology, Ecology and Evolution*, 1st ed., Springer, New York (1990).

[19] Banala, S. K. and Agrawal, S. K., "Design and Optimization of a Mechanism for Out-of-Plane Insect Winglike Motion with Twist," *Journal of Mechanical Design/Transactions of the ASME*, Vol. 127, pp. 841–844 (2005).

[20] McIntosh, S. H., Agrawal, S. K. and Khan, Z., "Design of a Mechanism for Biaxial Rotation of a Wing for a Hovering Vehicle," *IEEE/ASME Transactions on Mechatronics*, Vol. 11, pp. 145–153 (2006).

[21] Żbikowski, R., Galin´ski, C. and Pedersen, C. B., "Four-Bar Linkage Mechanism for Insectlike Flapping Wings in Hover: Concept and an Outline of Its Realization," *Journal of Mechanical Design/Transactions of the ASME*, Vol. 127, pp. 817–824 (2005).

[22] Żbikowski, R. and Galin´ski, C., "Insect-Like Flapping Wing Mechanism Based on a Double Spherical Scotch Yoke," *Journal of the Royal Society Interface*, Vol. 2, pp. 223–235 (2005).

[23] Information on http://www.festo.com/PDF_Flip/corp/smartbird_en/index.ftm (Festo's Smartbird).

[24] Yang, L. J., Huang, I. C., Chen, Y. S., Tang, W. T. and Wang, A. B., "A Parylene-LED Wingbeating Indicators for Visual Remote Sensing," *Technical Digest of the 16th International Conference on Solid-State Sensors, Actuators, and Microsystems*, Beijing, pp. 422–425 (2011).

[25] Yang, L. J., U.S. Patent 8,033,499B2 (2011).

[26] Information on http://www.ornithopter.org/ and its on-line store http://www.flyabird.com/index2.html.

[27] Mueller, T. J., "Aerodynamic Measurements at Low Reynolds Numbers for Fixed Wing Micro-Air Vehicles," *RTO AVT/VKI Special Course on Development and Operation of UAVs for Military and Civil Applications*, VKI, Belgium, p. 1 (1999).

[28] Rae, Jr., W. H. and Pope, A., *Low-Speed Wind Tunnel Testing*, 2nd ed., John Wiley & Sons Inc., New Jersey, p. 371 (1984).

[29] Lin, C. S., Hwu, C. and Young, W. B., "The Thrust and Lift of an Ornithopter's Membrane Wings with Simple Flapping Motion," *Aerospace Science and Technology*, Vol. 10, pp. 111–119 (2006).

[30] Yang, L. J., Kuo, A. F. and Hsu, C. K., "Wing Stiffness on Light Flapping Micro Aerial Vehicles," *Journal of Aircraft*, Vol. 49, pp. 423–431 (2012).

[31] Knoller, R., "Die Gesetze Des Luftwiderstands," *Flug-und Motortechnik (Wien)*, Vol. 3, pp. 1–7 (1909).

[32] Betz, A., "Ein Beitrag Zur Erklärung Des Segelfluges," *Zeitschrift für Flugtechnik und Motorluftschiffahrt*, Vol. 3, pp. 269–272 (1912).

[33] Weis-Fogh, T., "Quick Estimates of Flight Fitness in Hovering Animals, Including Novel Mechanisms for Lift Production," *The Journal of Experimental Biology*, Vol. 59, pp. 169–230 (1973).

[34] Pornsinsirirak, T. N., *Parylene MEMS Technology for Adaptive Flow Control of Flapping Flight*, Ph.D. Dissertation, Electrical Engineering, California Inst. of Technology, Pasadena (2002).

[35] Yang, L. J., Kao, C. Y. and Huang, C. K, "Development of Flapping Ornithopters by Precision Injection Molding," *Applied Mechanics and Materials*, Vol. 163, pp. 125–132 (2012).

[36] Kubo, Y., Shimoyama, I. and Miura, H., "Study of Insect-Based Flying Microrobots," *Proceedings of the IEEE Int. Conf. on Robotics and Automation*, Vol. 2, pp. 386–391, Atlanta, USA (1993).

[37] Vandenburghe, N., Zhang, J. and Childress, S., "Symmetry Breaking Leads to Forward Flapping Flight," *Journal of Fluid Mechanics*, Vol. 506, pp. 147–155 (2004).

[38] Alben, S. and Shelley, M., "Coherent Locomotion as an Attracting State for a Free Flapping Body," *Proceedings of National Academic Society of USA*, Vol. 102, pp. 11163–11166 (2005).

[39] Shyy, W., Berg, M. and Ljungqvist, D., "Flapping and Flexible Wings for Biological and Micro Air Vehicles," *Progress in Aerospace Sciences*, Vol. 35, pp. 455–505 (1999).

[40] Ho, S., Nassef H., Pornsinsirirak, N., Tai, Y.-C. and Ho, C.-M., "Unsteady Aerodynamics and Flow Control for Flapping Wing Flyers," *Progress in Aerospace Sciences*, Vol. 39, pp. 635–681 (2003).

[41] Greenewalt, C. H., "The Flight of Birds," *Trans. Am. Philos. Soc*., Vol. 65, pp. 1–67 (1975).

[42] Pennycuick, C. J., *Mechanical Constraints on the Evolution of Flight*, Vol. 8, pp. 83–98, In Padian K. (ed.) *The Origin of Birds and the Evolution of Flight,* Calif. Acad. Sci., San Francisco (1986).

[43] Pennycuick, C. J., *Mechanics of Flight*, Vol. 5, pp. 1–75, In Farner, D. S. and King, J. R. (eds.) *Avian Biology*, Academic Press, London New York (1975).

[44] Willmott, A. P. and Ellington, C. P., "Measuring the Angle of Attack of Beating Insect Wings: Robust Three-Dimensional Reconstruction from Two-Dimensional Images," *The Journal of Experimental Biology*, Vol. 200, pp. 2693–2704 (1997).

[45] Tang, W. T., Zhang, W., Huang, C., Young, M. and Hwang, I., "Postural Tremor and Control of the Upper Limb in Air Pistol Shooters," *Journal of Sports Science*, Vol. 26, pp. 1579–1587 (2008).

[46] Nguyen, T. T. and Byun, D., "Two-Dimensional Aerodynamic Models of Insect Flight for Robotic Flapping Wing Mechanisms of Maximum Efficiency," *Journal of Bionic Engineering*, Vol. 5, pp. 1–11 (2008).

[47] Ansari, S. A., Żbikowski, R. and Knowles, K., "Aerodynamic Modelling of Insect-Like Flapping Flight for Micro Air Vehicles," *Progress in Aerospace Sciences*, Vol. 42, pp. 129–172 (2006).

[48] Heathcote, S. and Gursul, I., "Flexible Flapping Airfoil Propulsion at Low Reynolds Numbers," *AIAA Journal*, Vol. 45, pp. 1066–1079 (2007).

[49] Zhao, L., Huang, Q., Deng, X. and Sane, S. P., "Aerodynamic Effects of Flexibility in Flapping Wings," *Journal of Royal Society Interface*, Vol. 7, pp. 485–497 (2010).

[50] Shyy, W., Aono, H., Chimakurthi, S. K., Trizila, P., Kang, C. K., Cesnik, C. E. S. and Liu, H., "Recent Progress in Flapping Wing Aerodynamics and Aeroelasticity," *Progress in Aerospace Sciences*, Vol. 46, pp. 284–327 (2010).

[51] Aono, H., Chimakurthi, S. K., Wu, P., Sallstrom, E., Stanford, B. K., Cesnik, C. E. S., Ifju, P., Ukeiley, L. and Shyy, W., "A Computational and Experimental Study of Flexible Flapping Wing Aerodynamics," *Proceeding of the 48th AIAA Aerospace Science Meeting*, Orlando, Florida, paper no. AIAA 2010-554 (2010).

[52] Wang, Z. J., "Two Dimensional Mechanism for Insect Hovering," *Physical Review Letter*, Vol. 85, pp. 2216–2219 (2000).

[53] Sun, M. and Tang, J., "Unsteady Aerodynamic Force Generated by a Model Fruit Fly Wing in Flapping Motion," *The Journal of Experimental Biology*, Vol. 205, pp. 55–70 (2002).

[54] Miao, J. M. and Ho, M.-H., "Effect of Flexure on Aerodynamic Propulsive Efficiency of Flapping Flexible Airfoil," *Journal of Fluids and Structures*, Vol. 22, pp. 401–419 (2006).

[55] Miao, J.-M., Sun, W.-H. and Tai, C.-H., "Numerical Analysis on Aerodynamic Force Generation of Biplane Counter-Flapping Flexible Airfoils," *Journal of Aircraft*, Vol. 46, pp. 1785–1794 (2009).

[56] Lua, K. B., Lim, T. T. and Yeo, K. S., "Effect of Wing-Wake Interaction on Aerodynamic Force Generation on a 2D Flapping Wing," *Experiments in Fluids*, Vol. 51, pp. 177–195 (2011).

[57] Suryadi, A. and Obi, S., "The Estimation of Pressure on the Surface of a Flapping Rigid Plate by Stereo PIV," *Experiments in Fluids*, Vol. 51, pp. 1403–1416 (2011).

Manuscript Received: Feb. 15, 2012
Accepted: May 4, 2012